Civil Engineering and Architecture 14(2): 692-708, 2026 http://www.hrpub.org
DOI: 10.13189/cea.2026.140204

Micropile Design Parameter Validation in Tropical Karst: A Case Study

Simon Kim Hui Law*, Norazzlina M.Sa'don, Abdul Razak Abdul Karim

Faculty of Engineering, Universiti Malaysia Sarawak, Malaysia

Received September 12, 2025; Revised December 25, 2025; Accepted January 12, 2026

Cite This Paper in the Following Citation Styles

(a): *[1] Simon Kim Hui Law, Norazzlina M.Sa'don, Abdul Razak Abdul Karim, "Micropile Design Parameter Validation in Tropical Karst: A Case Study," Civil Engineering and Architecture, Vol. 14, No. 2, pp. 692 - 708, 2026. DOI: 10.13189/cea.2026.140204.*

(b): *Simon Kim Hui Law, Norazzlina M.Sa'don, Abdul Razak Abdul Karim (2026). Micropile Design Parameter Validation in Tropical Karst: A Case Study. Civil Engineering and Architecture, 14(2), 692 - 708. DOI: 10.13189/cea.2026.140204.*

Abstract Micropiles are widely used in karstic limestone formations due to their ability to penetrate heterogeneous ground and provide reliable foundation support. However, uncertainties in design parameters for tropical karst environments, such as those in the Bau region of Kuching, Sarawak, remain underexplored. This study addresses the gap by validating micropile design assumptions against field performance through a case study of three micropiles installed in karst limestone. The research combines geotechnical site investigations, uniaxial compressive strength tests on rock cores, high-strain dynamic load tests using Pile Driving Analyzer (PDA), static maintained load tests up to 1300 kN, and load-transfer simulations. Results show that unconfined compressive strengths vary erratically with depth (mean 34-46 MPa), reflecting karst heterogeneity. Static tests indicate settlements of about 9.5 mm at 1300 kN, with extrapolated ultimate capacities ranging from 2390 kN to 4686 kN using Chin's method, far exceeding the design value of 1300 kN. PDA estimates (1429-1724 kN) confirm capacities above design, while simulations reveal contributions from soil shaft friction (182-226 kN) and end bearing (63-179 kN), ignored in conservative design. Rock socket friction mobilized lower than expected (140-165 kPa), likely due to epikarst weathering, construction factors, and limited test mobilization. The findings validate conservative design practices but highlight load-sharing mechanisms in karst, including non-negligible soil and base resistance. This study recommends combining dynamic and static tests with simulations for optimized designs, filling local and global knowledge gaps in micropile performance.

Keywords Karst, Micropiles, Pile Load Test, Pile Driving Analyzer (PDA), Maintained Load Test (MLT)

1. Introduction

Micropiles are small-diameter drilled and grouted piles [1]. This solution is widely used due to the good performance of its ability to bond through complex layers [2]. Unlike driven piles, micropiles are adaptable in heterogeneous ground conditions [3]. Undulating bedrock profile, pinnacles, and voids are the characteristics of karstic limestone formation [4]. In such settings, micropiles are often the robust and preferred foundation system [5]. Even with the wide use of micropiles in these areas, many uncertainties remain [5]. In particular, it is unclear if design methods for normal soil and rock apply [6]. Engineers often use extra safety factors or lower values to handle karst risks [7]. Static Maintained Load Tests, commonly regarded as the gold standard for field verification, are typically conducted on a smaller number of piles due to cost constraints [8]. Design engineers seldom compare the proposed designs with field observations [9], often due to project management pressure prioritizing site progress over technical validation, which is typically seen as unproductive and limited to academic research. This creates a significant gap between design and actual performance.

Limited research exists on micropile performance in tropical karst limestone in Bau, Kuching. Few studies compare design with field results [4, 5]. Engineers often verify load tests and proceed without further analysis [4]. Limited studies have compared micropile design with comprehensive load and dynamic tests in Bau's karst limestone. Micropile behavior in karst may differ from standard conditions, and existing guidelines, suited for uniform ground, may not apply. This paper focuses on the case of Bau, Kuching, to connect design assumptions with field outcomes and evaluate the Pile Driving Analyzer (PDA) for assessing pile capacity in karst. For the Sarawak region, this study investigates the suitability of current methods for tropical karst and analyzes load transfer. The findings are to improve the local knowledge gap and to contribute to global understanding. The main aims of this study are to assess the ability of current design methods and parameters to accurately reflect the behavior and load transfer of micropiles in tropical karst regions. This study not only fills a local gap but also adds a case study to the global literature on micropile performance in karst.

2. Literature Review

Micropiles are small-diameter piles, ranging from 100 mm to 300 mm diameter, drilled, reinforced with bars or pipes, and filled with grout [2]. Reinforcement can be a central bar or steel casing like API pipes [2]. The outer part can have a permanent or temporary casing [4]. Micropiles are commonly used due to their high versatility and ability to be installed in restricted access, low headroom, or complex geological settings, such as karstic formations [2].

Micropiles are often chosen in karst areas because they can penetrate complex layers [2]. With casing, they can cross voids with little grout loss. The casing seals voids and unstable zones. This lets them reach solid rock under weak areas. While micropiles work well in hard spots, larger bored piles may be better in even ground [2]. Uncased bored piles in karst risk fluid loss and hole collapse in cavities [10]. Uncased micropiles face similar issues [4, 5]. Casing is key for reducing grout loss, preventing collapse, and ensuring good bonding [4].

Micropiles get the most load capacity from grout-ground contact along their length, which is called shaft friction [1, 5]. End bearing is usually seen as small [5]. Local practice often ignores soil shaft friction and focuses on rock-grout bond [10]. End bearing is also ignored due to risks from hidden voids under the tip [10]. Dotson [1] highlighted that unseen voids beneath the bedrock can challenge conventional deep foundations, such as bored piles and driven piles. In contrast, fully grouted micropiles offer a more secure alternative, as they bond into the rock and span across the unstable zone. Unlike driven piles, micropiles avoid imposing a significant point load on bedrock that might contain cavities [5].

Dotson [1] noted that micropile success in karst varies due to uncertainties in grout bond and load spread. Drilling and grouting methods affect bond and pile strength. Choose methods carefully for reliability in karst. For example, pressure grouting versus gravity grouting changes bond strength. High pressure can crack intact rock. In air-filled cavities without casing and low grout pressure, capacity drops. Use tremie grouting or casing to fix this. If needed, add post-grouting to improve the bond. Gómez [11] performed static load tests and found that PDA results matched static tests well. This shows PDA can check micropile capacity. However, 5% of piles can not reach working load, and 30-50% lack a safety factor of 2. This shows variability that can be due to poor bonding or voids. This study compares test results with designs to check empirical and analytical methods.

Most literature on micropiles in karst focuses on ultimate capacity, but service limits like settlement are often missed. Settlement can make structures unusable even if the capacity is high. It is necessary to check service limits on complex ground. This study looks at both capacity and settlement curves with models. This gives a better understanding of micropile behavior in tropical karst. It helps improve design and evaluation. Recent studies on karst geohazards emphasize the role of rapid dissolution in tropical environments, leading to unpredictable cavities and sinkholes that exacerbate uncertainties in micropile design [12, 13]. Geophysical methods, such as ERT (Electrical Resistivity Tomography) and remote sensing, are recommended for detecting hidden features to refine site investigations [14, 15]. Case studies from Malaysia highlight adaptive strategies like grouting and soil mixing to mitigate groundwater instability in limestone formations [16, 17]. Failure mechanisms in karst underscore the need for integrated approaches to ensure foundation stability [18, 19]. These insights support conservative practices while identifying opportunities for optimized load transfer in heterogeneous grounds [9, 20].

In order to install micropiles, the ODEX system is used to drill through the soft overburden. The casing is pushed down during the process to prevent collapse. Then, the DTH (Down The Hole) hammer or duplex system is mobilised to drill into the competent limestone. Once the borehole reaches the required depth, water or air is flushed out to remove loose cuttings and ensure a clean rock socket. API pipe reinforcement combined with centralizers is then installed into the borehole. Next, cement grout is poured from the bottom upward using a tremie pipe to form a continuous column, ensuring proper socket contact. After grouting, the pile is kept to cure with the head protected to maintain its strength.

3. Methodology

This investigation is developed in order to study the

performance of micropiles installed through a comprehensive programme of laboratory experiments, dynamic load testing, static load testing, and numerical back analysis. Notably, the author supervised the field activities, including the site investigations, the rock core sampling, the dynamic load tests, and the static maintained load tests. The methodology of the investigation is structured in such a way that both independent and cross verification of the assessment of the pile can be conducted, with particular focus on evaluating the performance of the micropiles under serviceability and ultimate limit states.

The geotechnical site investigation and rock core sampling aim to characterize the subsurface conditions and determine the strength and quality of the rock. Significant karstic cavities were observed during the investigation, and these findings were documented accordingly. Following the rock core sampling, these core samples were retrieved and subjected to uniaxial compressive strength tests.

Since karst voids and cavities were discovered during the site investigation, the micropiles were designed with permanent outer diameter steel casings to bridge through the overburden soil layers filled with cavities and prevent excessive grout loss into the cavities. From the uniaxial compressive strength tests, the micropiles were designed based on rock shaft friction with a 6-meter socket into the limestone stratum. Furthermore, to ensure no cavities beneath the pile toes, pilot holes were drilled to an additional 10 meters below the planned founding level of the micropiles.

Three micropiles were selected for detailed scrutiny for this case study, with the parameters presented in Table 1. Firstly, high-strain dynamic load testing was performed on these micropiles (Figure 1). And the intention was to evaluate their capacity and load distribution. This test was conducted through restrike tests after a minimum setup period of three weeks after micropile installation. During these restrike tests, a drop hammer was used to strike the pile head, thus generating a high-strain stress wave that traverses the entire pile length. The Pile Driving Analyzer equipment was attached close to the pile head in order to record the strain and acceleration resulting from the hammer impact. The plan for at least three weeks of setup period was to allow any excess pore water to dissipate and for the soil strength at the soil-pile interface to recover. This is crucial for the soils to achieve an acceptable bond with the grout. The dynamic measurements from the hammer blow were initially analyzed based on the Case Method. Subsequently, signal matching technique analysis, using CAPWAP analysis, was used to interpret the dynamic response from the stress wave propagation and estimate the equivalent static load resistance behaviour mobilized during the hammer impact. This analysis provided an estimate of ultimate pile capacity as well as the distribution of resistance along the shaft and the end bearing. Multiple hammer blows were applied and analyzed to ensure consistency. The PDA restrike method was chosen because it allows for a quick assessment of ultimate pile capacity and provides insight into shaft friction and end bearing contributions by analyzing the force-velocity response. All PDA tests were conducted prior to the static maintained load tests to avoid overstressing the piles.

Table 1. Parameters of micropiles selected for detailed scrutiny

Pile parameters	Pile A2-2	Pile A1-11	Pile H2-1
Length of Pile (m)	25.3	27.0	30.0
Diameter of Pile (m)	0.3	0.3	0.3
Socket Length (m)	6.0	6.0	6.0
Casing Length (m)	19.3	21.0	24.0
Length of Pile in Soil (m)	11.8	12.8	12.0
Length of Pile in Rock (m)	13.5	10.4	18.0
Cavity found at depth (m)	15.2 - 17.5	16.3 - 19.5	14.0 - 16.5, 18.5 - 24.0

Subsequently, these micropiles were further tested through static maintained load tests using a kentledge system. A reaction platform was constructed by stacking concrete blocks on top of a load frame, and a hydraulic jack was attached to the pile head to jack against the load frame. The schematic diagram of the static load test setup is illustrated in Figure 2. The safe working load of the micropiles was 650kN. The loading procedure and steps adhere to the JKR (Jabatan Kerja Raya) guidelines, with a load increment of 25%. Settlement readings were recorded at each stage. Each pile was subjected to two loading cycles. In the first cycle, the load was applied once at the safe working load and then gradually removed to zero to assess the plastic deformation. In the second cycle, the pile was reloaded incrementally beyond the first cycle's peak load, up to twice the safe working load, and progressively unloaded to obtain the permanent plastic deformation. As none of the piles reached a definitive plunging failure at 1300kN, the ultimate pile capacities were estimated through extrapolation. Specifically, Chin's hyperbolic extrapolation method was applied to the load settlement data to predict each pile's asymptotic ultimate pile capacity. This method involves plotting settlement with applied pile load against settlement and fitting a linear regression line to estimate the ultimate pile capacity, providing a rational basis for the inferred ultimate pile capacity beyond the maximum applied load. Using two load cycles, including a reload beyond the same peak load from the first cycle, facilitates the assessment of residual settlement after removing the test load.

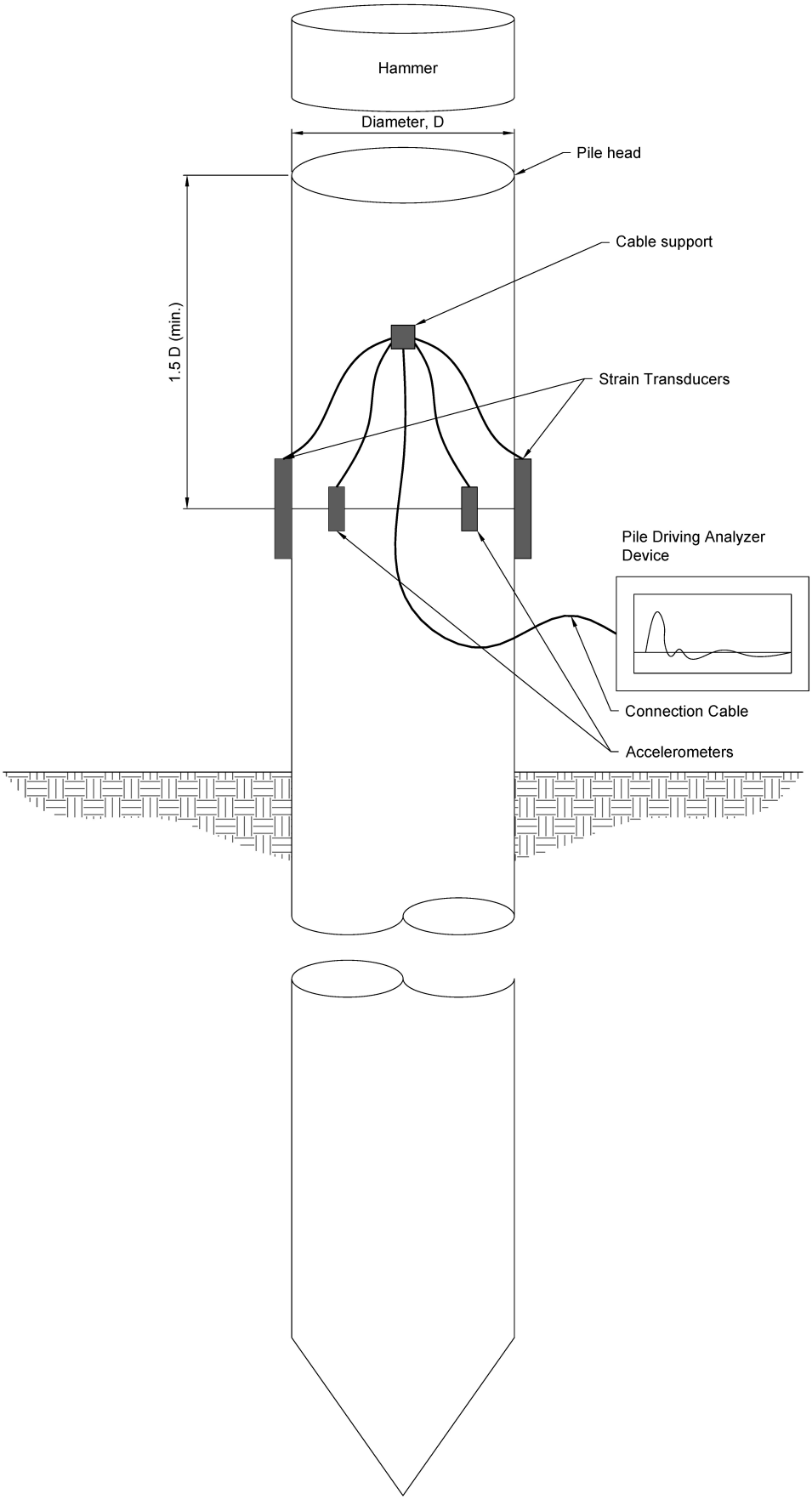

Figure 1. Schematic diagram of the dynamic load test setup

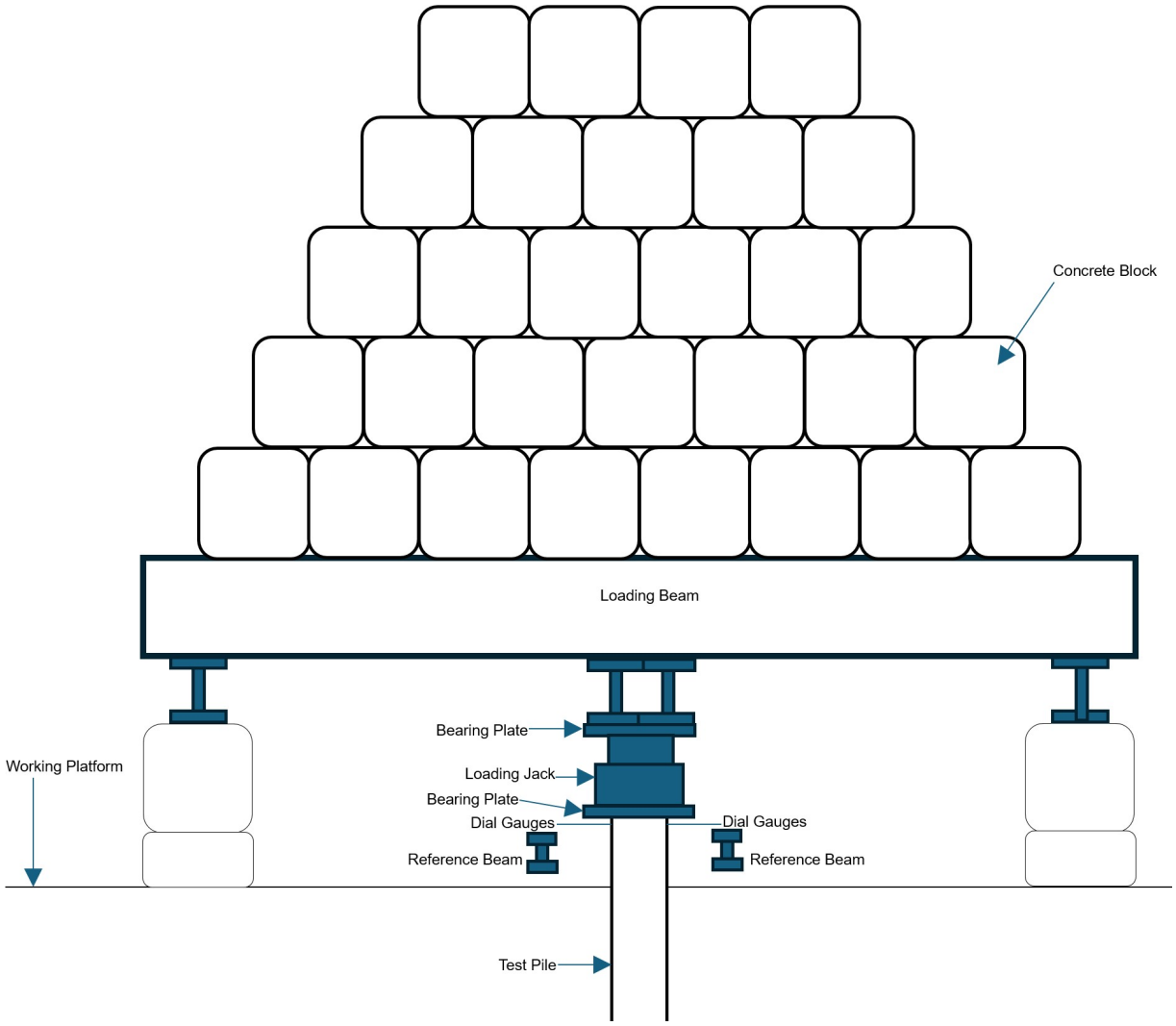

Figure 2. Schematic diagram of the static maintained load test setup

In addition to field testing, analytical simulations were conducted to model the pile load-settlement behavior. The load-transfer approach was employed using two distinct software packages, including TZPILE and UniPile. These programs simulate axial static load tests by representing soil/pile interaction through nonlinear springs: t-z curves for shaft friction along the pile and q-z curves for end bearing. The t-z curves represent the nonlinear relationship between the unit shaft friction (t) and the local pile displacement (z) along the pile shaft, typically modeled using hyperbolic or bilinear functions to capture elastic-plastic behavior. Similarly, q-z curves describe the end-bearing resistance (q) as a function of toe displacement (z), often using a hyperbolic form. Site-specific soil and rock parameters, derived from geotechnical investigation, were used as the initial input. The software can generate load-transfer curves internally for specified soil layers or accept user-defined curves. In this study, the t-z and q-z curves were calibrated to match the observed test behavior. As mentioned, the simulations utilized the initial geotechnical design parameters as input, which conservatively disregarded any shaft friction in the overlying soils and attributed capacity solely to the rock socket's shaft friction. The model for each pile was subsequently refined by adjusting the side friction and end bearing parameters until the computed load-settlement response closely aligned with the field results from the static load tests. This calibration process was iterative. After calibrating these curves, a site-specific load transfer relationships were established to reproduce the measured pile behaviour. These calibrated models can then be used to examine the load distribution along the pile and predict pile performance under different loading scenarios. The integration of field tests with analytical t-z/q-z modeling offers a comprehensive methodology. In this context, static tests provide a direct measure of performance, dynamic tests offer rapid capacity assessment and insight into resistance distribution, and simulations enable more in-depth interpretation and the generalization of findings to different conditions.

4. Results and Discussion

Figure 3 illustrates the results of unconfined compressive strength (UCT) tests performed on rock core samples retrieved from multiple boreholes. The results were recorded for 12 different boreholes with depths ranging from 6.5 m to 31 m. Overall, the UCT values of the BH group (BH1 - BH5) are slightly larger than those of the ABH group (ABH1 -ABH7), with mean values of 46 MPa and 34 MPa, respectively. As shown in the figure, the values of the unconfined compressive test for the BH group appear to be larger than those for the ABH group, with the maximum value being 75 MPa for BH1 (at 13-m depth). Meanwhile, the maximum value of ABH is 72 MPa at ABH7 (at 22-m depth). This erratic scatter, devoid of a clear depth-dependent trend, exemplifies the inherent heterogeneity of karstic terrains, where localized weathering, fractures, solution features, and infilled voids disrupt the performance of uniform rock mass properties, thereby introducing considerable geotechnical uncertainty in foundation design and predictions.

Figure 4a presents the comparison between the simulated load-settlement curve obtained from shaft load-transfer (t-z) and base load-settlement (q-z) models and the actual measured settlement for micropile A2/2 during static maintained load testing. As can be seen in the figures, a close alignment between the two values is presented, particularly at lower loads. When the applied loading reaches 1300 kN, a minor difference of 6.6% is noted, as the simulation estimates slightly greater settlement. This correlation validates the efficacy of the load-transfer back-analysis in replicating the observed behavior, highlighting the mobilization of shaft friction in the rock socket as the primary resistance mechanism, while also revealing modest contributions from overlooked soil friction and end bearing, consistent with the conservative design assumptions in karstic formations.

For cases of micropiles A1/11 and H2/1, as presented in Figure 4b and Figure 4c, the trends of the simulations and the measurements remain consistent, with the simulated results predicting slightly larger settlements. Moreover, the final settlement values for all three cases show slight variation, converging around a mean value of approximately 9.5 mm at the maximum applied load of 1300 kN.

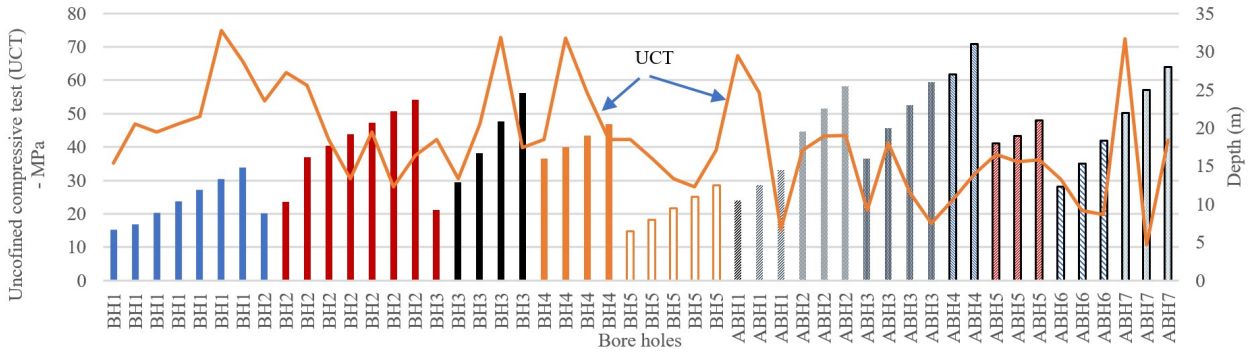

Figure 3. Variation of unconfined compressive strength (UCT) with depth for rock core samples

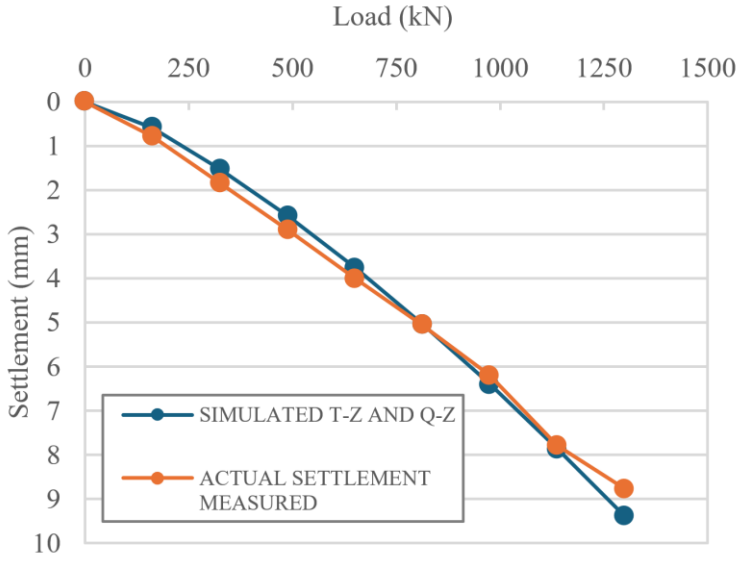

(a)

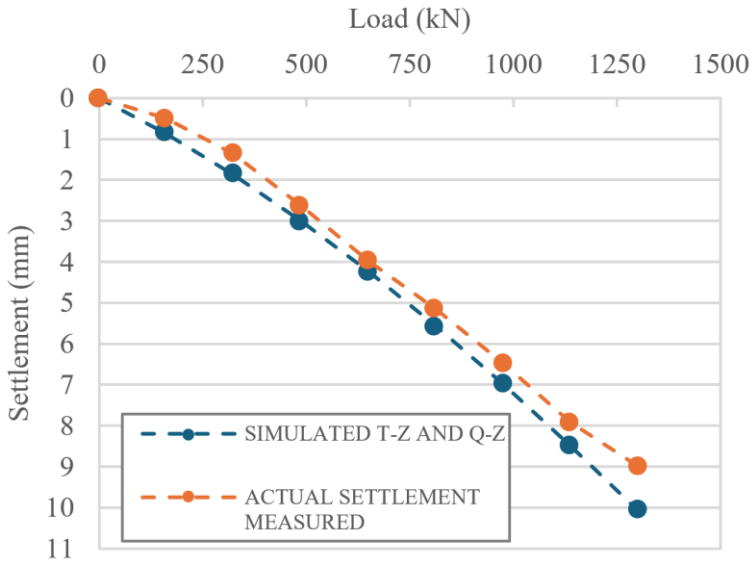

(b)

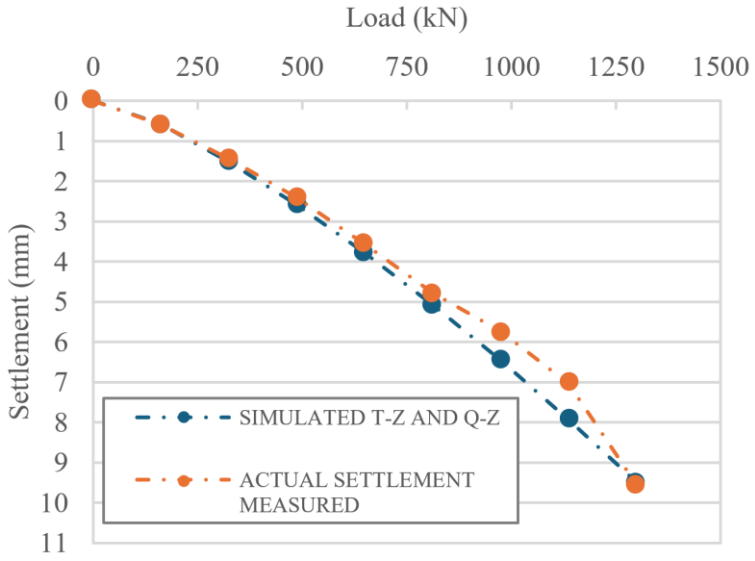

(c)

Figure 4. Comparison between simulated and measured settlement under loading for Piles A2/2 (a); Pile A1/11 (b); Pile H2/1 (c)

Figure 5a presents the relationship between the unit load transfer (t-z) and displacement for micropile A2/2. The residual soil layer (0.0-19.3 m) shows negligible shaft resistance (10 kN/m^2), showing that the soil friction is insignificant. In contrast, the rock socket (19.3-25.3 m) mobilized substantial resistance, with an ultimate unit shaft resistance of about 140 kN/m^2 at 0.05 m of maximum displacement. Indeed, the displacement increases slowly in the initial stage as the unit load transfer rises from 0 to about 100 kN/m^2. Then, the displacement of the rock socket increases more sharply as the load transfer increases from 100 kN/m^2 to 140 kN/m^2. This behavior reflects typical grout-rock interface characteristics, confirming that pile capacity is governed primarily by the rock socket, while soil friction provides only a minor contribution.

The ultimate unit load transfer value of pile A2/2 was compared with those of pile A1/11 (Figure 5b) and pile H2/1 (Figure 5c). It can be observed that pile H2/1 exhibited the highest ultimate resistance at 165 kPa, followed by pile A1/11 at 150 kPa, both exceeding the critical value of 140 kPa obtained for pile A2/2. In addition, the overall deformation trends concerning unit load transfer appear consistent across all three piles, indicating similar load-displacement behavior despite differences in ultimate capacity.

Figure 6 depicts the base resistance-displacement (q-z) relationship of piles A2/2, A1/11, and H2/1, respectively. For the case of pile A2/2, the curve indicates an ultimate base resistance of approximately qult = 8000 kPa, mobilized at a reference displacement of about z_{50} = 15 mm. The response shows a progressive increase in resistance with increasing settlement. The initial stage (z < 5 mm)

demonstrates a relatively stiff response with rapid mobilization of toe resistance, followed by a gradual reduction in stiffness beyond 10 mm as the load approaches the asymptotic ultimate value.

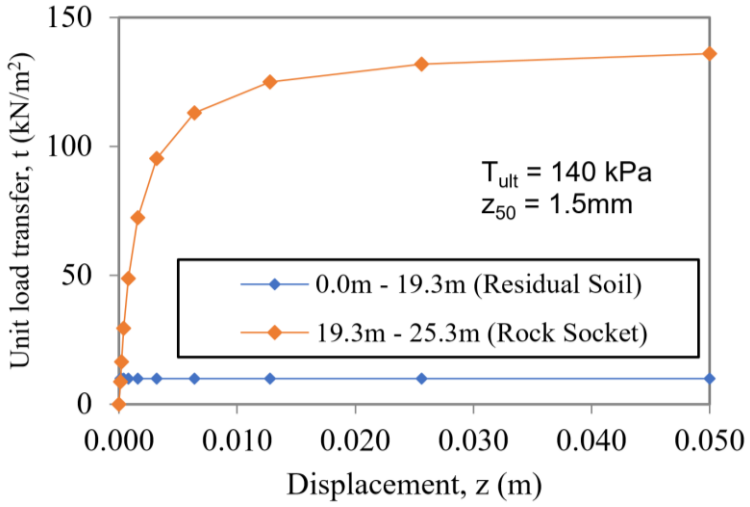

(a)

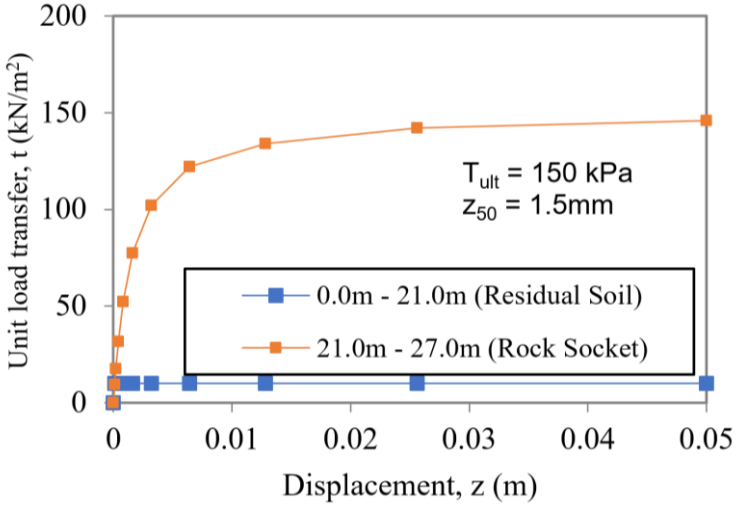

(b)

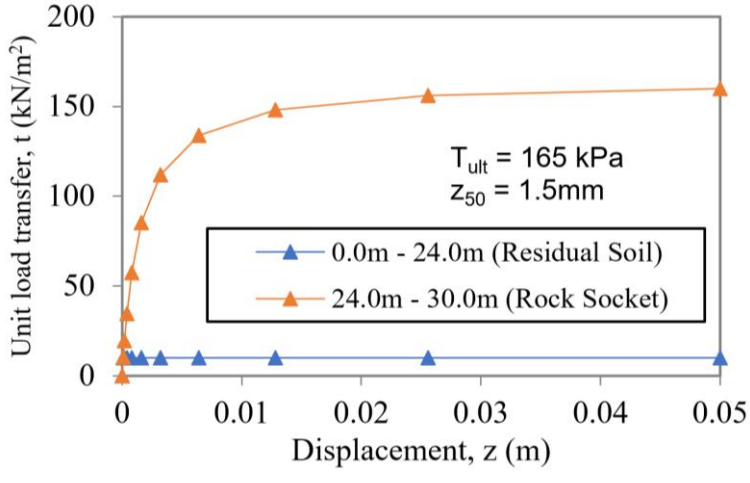

(c)

Figure 5. Displacement development corresponding to unit load transfer for Piles A2/2 (a); Pile A1/11 (b); Pile H2/1 (c)

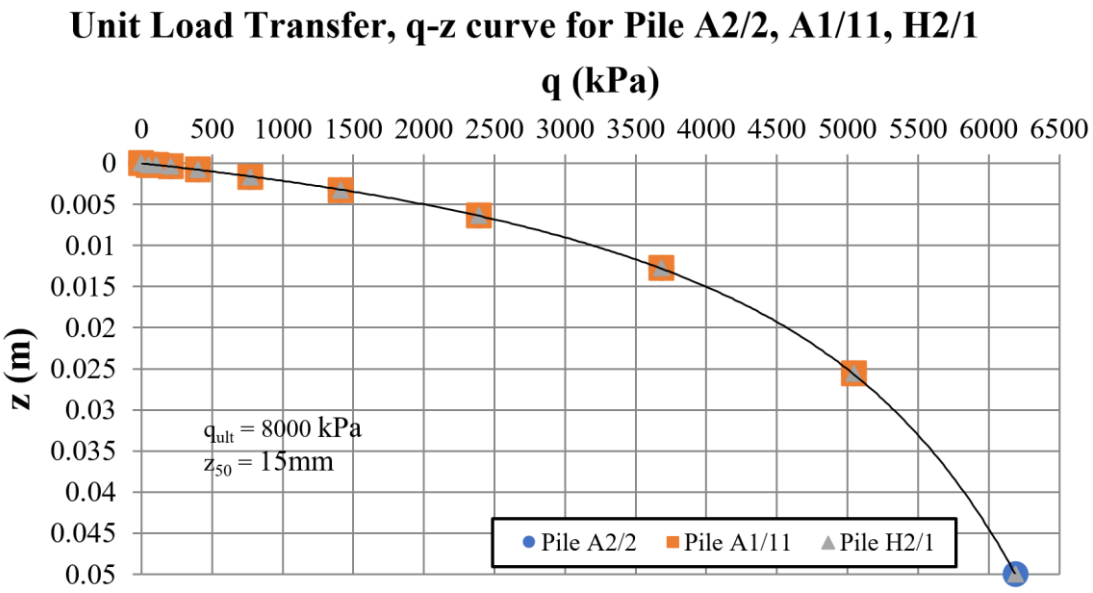

Figure 6. Relationship between unit load transfer and depth for Piles A2/2, Pile A1/11, Pile H2/1

This behavior reflects the typical characteristics of end-bearing resistance in rock-socketed micropiles, where a larger displacement is required to mobilize base resistance compared to shaft friction fully. Compared with the t-z response, the q-z curve emphasizes that while the rock socket shaft friction governs performance at small displacements, the pile base provides a significant reserve capacity that becomes mobilized only at larger settlements. This supports the conservative design approach, where end bearing was excluded. Field behavior confirms its potential contribution under higher load levels.

One notable finding from the rock socket's lateral adhesion proved far weaker than projected, dipping below even the scaled-back estimate, halved from the assumed maximum that guided the blueprints. One possible reason is that the tests did not reach full failure. Ending at fixed limits leads to measuring only part of the bond strength at the noted displacement, without causing total collapse. Other reasons relate to the socket placement in epikarst limestone. This weathered upper layer has rough surfaces, cracks, clay fills, and voids. Though roughness might suggest higher bond from interlocking and dilation, the weak or crumbly rock reduces interface strength. Soft spots or clay layers fail early and crush asperities under low pressure. Construction errors, such as leftover debris, smears, or poor socket cleaning and roughening, could make this worse and create an interface weaker than planned.

A scale effect may also add to this difference. Lab tests or studies on smaller-diameter piles often show higher unit side friction in rock, but full-scale piles tend to have lower values. This happens because larger diameters include more rock mass variation and are less able to mobilize even friction across the whole interface. Also, a bigger socket needs more absolute displacement to achieve the same strain at the interface. If design predictions came from ideal or small-scale conditions, the real full-scale behavior could mean lower efficiency. In short, the mix of weathered rock socket, possible construction issues, and scale-based mobilization caused the observed rock-socket friction to be below the conservative design estimate. This result highlights the value of site-specific testing as it confirms the design works well, and it gives an understanding of actual performance to improve future designs or construction steps.

Load-settlement response during static maintained load testing for different piles is presented in Figure 7 under two loading cycles. Regarding micropile A2/2 (Figure 7a), the first cycle shows a non-linear increase in settlement with applied load up to 650 kN, reaching approximately 3.79 mm at peak, followed by unloading with residual deformation of about 0.58 mm. The second cycle shows a stiffer reload path due to prior consolidation, but similar non-linear behavior at higher loads, culminating in a total settlement of around 9.35 mm at 1300 kN before remaining deformation is 2.63 mm under unloading. This pattern reveals dominant elastic recovery in the initial cycle and progressive plastic deformation in the reload, affirming the pile's robust capacity in karstic limestone with mobilized rock socket friction exceeding design assumptions, while highlighting minimal contributions from soil layers and end bearing at tested displacements. For piles A1/11 and H2/1, as presented in Figure 7b and Figure 7c, respectively, peak settlement values show no difference between the two loading cycles; however, the second cycle shows settlement recovery closer to the initial value.

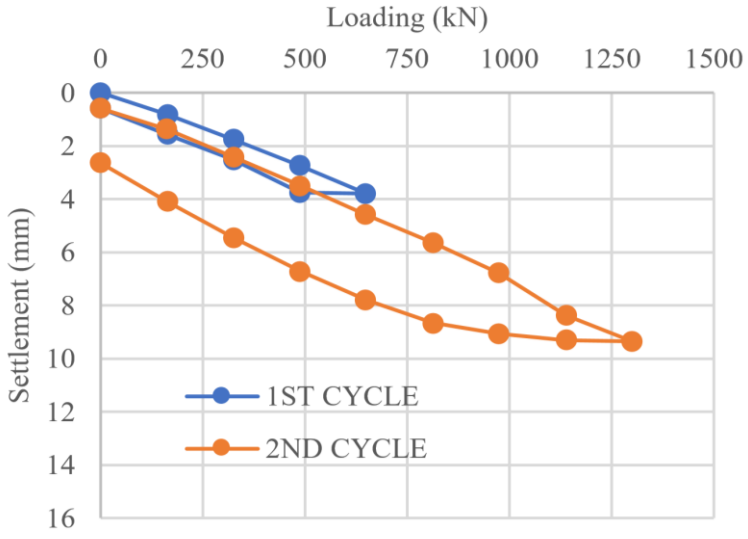

(a)

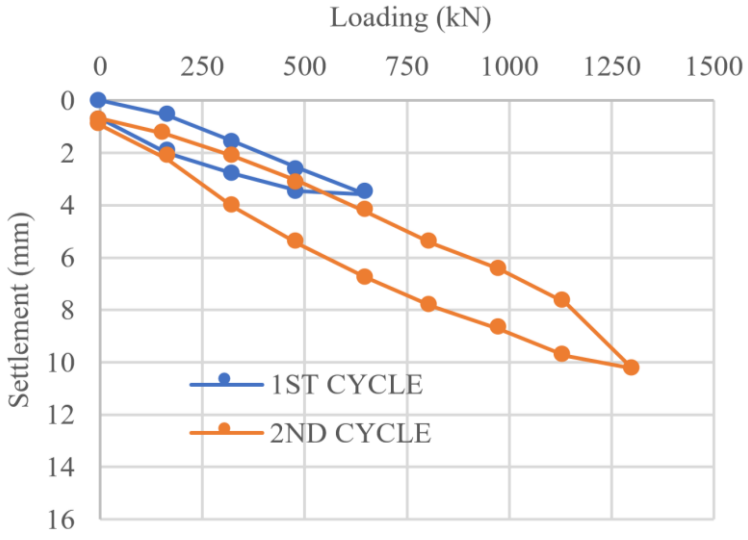

(b)

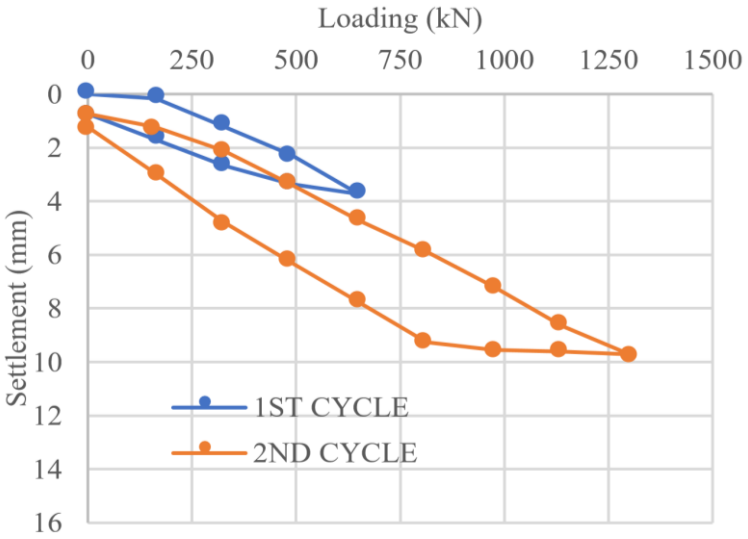

(c)

Figure 7. Load-settlement curves during static maintained load testing for Piles A2/2 (a); Pile A1/11 (b); Pile H2/1 (c)

Figure 8a illustrates the Chin-Kondner extrapolation plot for micropile A2/2, resulting from the load-settlement data obtained during the static maintained load test. In this method, the settlement to applied load ratio has a linear regression fit of y = 0.234x - 5.0971 with a good correlation coefficient (R^2 = 0.868). The slope (m = 1/Qult) corresponds to the reciprocal of the ultimate capacity (Qult = 4686 kN), while the negative intercept reflects the initial elastic response and potential non-linearities at low loads. Similarly, Figure 8b presents the Chin-Kondner plot for micropile A1/11, with a linear regression of y = 0.4184x - 3.7377 and a moderate correlation (R^2 = 0.8416). The extrapolated ultimate capacity is estimated as Qult = 2.390 MN, which, despite the lower R^2 value suggesting some scatter possibly attributable to heterogeneous rock quality or variable grout bonding in the epikarst zone, still confirms a capacity surpassing the design nominal resistance. Figure 8c depicts the Chin-Kondner extrapolation for micropile H2/1, showing a regression line of y = 0.3647x - 3.8857 with a high correlation (R^2 = 0.9503). The derived ultimate capacity is estimated as Qult = 2.742 MN. The high R^2 value supports reliable extrapolation in this context.

In the design phase, a cautious approach was used to estimate pile capacity. The shaft friction in the overlying soil and the end-bearing resistance at the pile base were excluded from calculations, assuming these were unreliable or hard to fully engage under service conditions. Ignoring soil shaft friction and base resistance is often advised for bored piles socketed into rock, especially when construction issues might hinder their full engagement. By omitting these, the design relied only on rock-socket side friction to bear the load, applying a higher safety factor to address uncertainties. Specifically, the rock-socket shaft friction was reduced to about half its expected value in design calculations. This aligns with standard practice to ensure a sufficient safety margin against failure. This reflects the understanding that, despite high ultimate shaft resistance suggested by intact rock strength and interface roughness, not all resistance is engaged in service without excessive movement, so the design credits only a portion to meet safety and serviceability requirements.

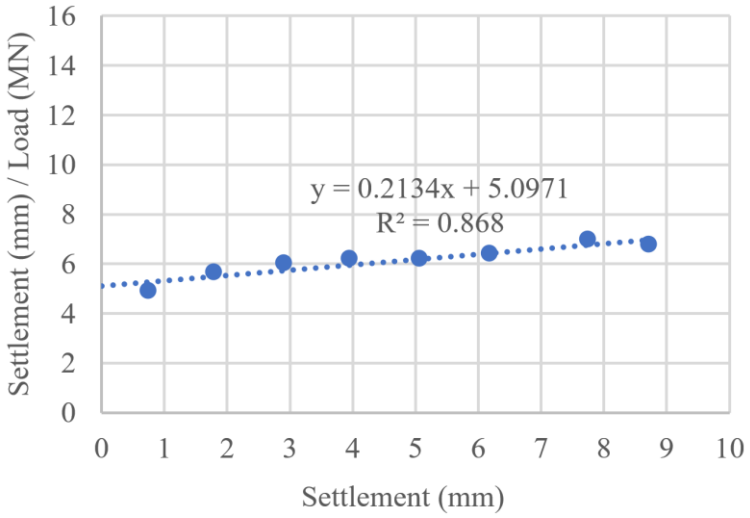

(a)

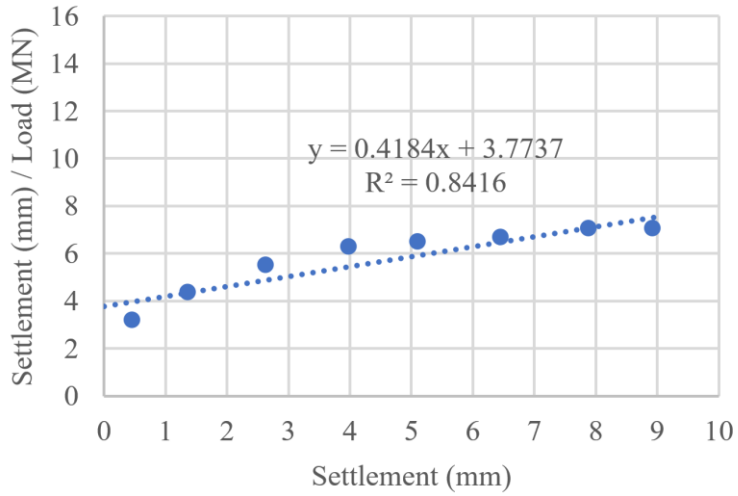

(b)

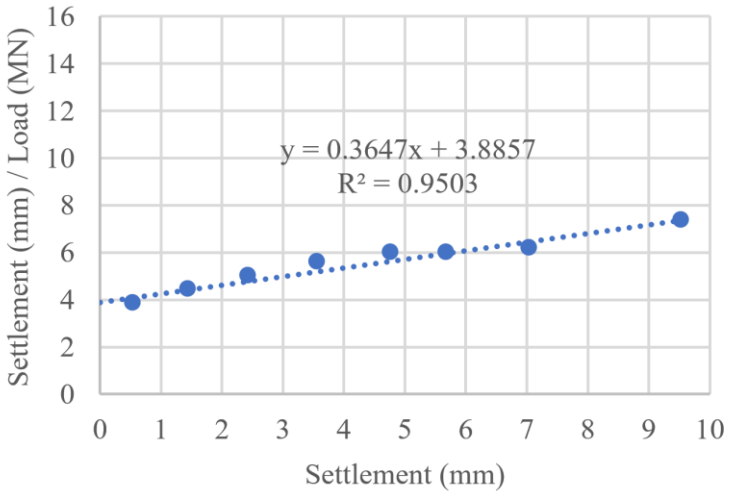

(c)

Figure 8. Chin-Kondner extrapolation plots for ultimate capacity estimation of Piles A2/2 (a), A1/11 (b), and H2/1 (c)

However, pile load testing showed that the previously ignored components, soil shaft friction and base resistance, were not zero. They contributed measurable resistance to the pile's capacity, though not accounted for in the design. In hindsight, this is unsurprising: as the pile is loaded, some shear stress develops along the shaft in soil, and the base carries some load with sufficient settlement, unless these interfaces are fully slipped or separated. The design's assumption to ignore them was a cautious simplification to ensure the rock socket alone could carry the load with ample safety. Test results confirmed that the rock socket provided most of the capacity but also showed that the overburden soil and base resistance offered additional reserve, partially engaged during testing. The tests highlight that real behavior is more complex, with load shared among all pile-soil system components.

Table 2 summarizes A2-2 performance: design conservatively attributes 1300 kN solely to rock shaft friction (1413.7 kN); PDA yields 1724 kN with superior soil shaft (1503 kN) but modest end (221 kN); Chin extrapolation estimates ultimate at 4686 kN, surpassing counterparts; t-z/q-z simulation at 1300 kN apportions soil shaft (181.9 kN), rock shaft (939.2 kN), and end (178.9 kN), revealing overlooked contributions. It correlates well with Figures 2a-6a, validating conservatism.

Table 3 presents the load performance analysis for A1-11: design mirrors 1300 kN from rock shaft; PDA totals 1428.9 kN with lower soil shaft than A2-2 but higher end; Chin yields 2390.1 kN ultimate, the weakest among tested piles; simulation distributes soil shaft, rock shaft (973.5 kN), and end (128.6 kN). It aligns with Figures 2b and 6b, indicating heterogeneous mobilization.

Load test results for pile H2-1 are presented in Table 4: design consistent at 1300 kN rock shaft; PDA sums 1502.7 kN with intermediate soil shaft and end; Chin extrapolates 2742 kN ultimate, exceeding A1-11 but below A2-2; simulation assigns the highest soil shaft (226.2 kN) and rock shaft (1010.8 kN) but the lowest end (63 kN). It relates to Figures 2c and 6c, highlighting the soil's variable yet non-negligible role in karst.

The comparison of the different test methods - namely the high-strain dynamic test (PDA test), the static maintained load test (MLT), and the t-z/q-z back-analysis of the static test data - offers a valuable perspective on pile performance. These methods gave different capacity and load distribution results but are complementary, offering a fuller picture of pile behavior under load. The PDA test, involving pile striking and stress wave analysis, such as CAPWAP, estimated total capacity (side + base) from dynamic response. Dynamic tests often show higher capacity than static tests due to strain-rate effects boosting soil resistance and signal-matching analysis estimating equivalent static capacity. PDA results indicated an ultimate capacity above the design load, suggesting the pile would not fail at target loads. However, dynamic tests have uncertainties, such as assuming fully mobilized resistance in a brief impact and estimating damping, leading to varied capacity predictions. Thus, while PDA provided an upper-bound estimate, it needed static test validation for reliable, service-focused data.

On the other hand, the MLT applied load gradually, measuring pile movement under sustained loads. It directly showed pile-soil system behavior up to the maximum test load (likely above the working load but below failure to protect the pile). The MLT's load-settlement curve revealed mobilized capacity at the test limit and pile stiffness. The disparity between the apparent capacity derived from PDA and the stopping load of MLT does not suggest a contradiction, as it indicates that the MLT did not reach the point of geotechnical failure, whereas the PDA estimated the ultimate failure capacity. The MLT confirmed that at the design load and higher proof loads, settlement stayed within acceptable limits with no geotechnical failure. It offered a direct, safe measure of capacity and performance up to a specific load, while PDA estimated the likely failure load.

Table 2. Load test results for pile A2-2

Determination method	Shaft Friction (kN)		End Bearing in Rock (kN)	Total Capacity (kN)
Based on Design	Soil:	Ignored	Ignored	1300.0
	Rock:	1413.7		
Based on PDA	Soil:	1503	221	1724.0
	Rock:	1503		
Based on Static Maintained Load Test	Soil:	Ignored	Ignored	4686.0
	Rock:	Ignored		
Simulated Load Settlement Curve based on t-z and q-z analysis	Soil:	181.9	178.9	1300.0
	Rock:	939.2		

Table 3. Load test results for pile A1-11

Determination method	Shaft Friction (kN)		End Bearing in Rock (kN)	Total Capacity (kN)
Based on Design	Soil:	Ignored	Ignored	1300.0
	Rock:	1413.7		
Based on PDA	Soil:	856.4	572.5	1428.9
	Rock:	856.4		
Based on Static Maintained Load Test	Soil:	Ignored	Ignored	2390.1
	Rock:	Ignored		
Simulated Load Settlement Curve based on t-z and q-z analysis	Soil:	197.9	128.6	1300.0
	Rock:	973.5		

Table 4. Load test results for pile H2-1

Determination method	Shaft Friction (kN)		End Bearing in Rock (kN)	Total Capacity (kN)
Based on Design	Soil:	Ignored	Ignored	1300.0
	Rock:	1413.7		
Based on PDA	Soil:	1042.0	460.7	1502.7
	Rock:	1042.0		
Based on Static Maintained Load Test	Soil:	Ignored	Ignored	2742.0
	Rock:	Ignored		
Simulated Load Settlement Curve based on t-z and q-z analysis	Soil:	226.2	63.0	1300.0
	Rock:	1010.8		

Figure 9a illustrates the comparison between the ultimate pile capacities derived from high-strain dynamic load tests (PDA) and those extrapolated from static maintained load tests (MLT) using Chin's method for the three micropiles (A2/2, A1/11, and H2/1). The data points fall below the line of equality, indicating that the MLT extrapolated capacities are substantially higher than the PDA estimates across all tested piles. This finding reverses the typical observation in the literature, where PDA results often exceed MLT capacities due to strain-rate effects and dynamic mobilization.

Figure 9b compares the shaft friction resistances estimated from high-strain dynamic load tests (PDA) and those obtained through calibrated t-z load-transfer back-analysis for the three micropiles (A2/2, A1/11, and H2/1). The data points are scattered around the line of equality, revealing a mix of overprediction and underprediction by the PDA method relative to the t-z-derived values. Specifically, for piles A2/2 and A1/11, the PDA estimates exceed the t-z shaft frictions (points above the line), whereas for pile H2/1, the PDA underestimates the shaft friction (point below the line).

Figure 9c compares the end bearing resistances estimated from high-strain dynamic load tests (PDA) and those derived from calibrated q-z load-transfer back-analysis for the three micropiles (A2/2, A1/11, and H2/1). The data points are positioned well above the line of equality, revealing a consistent and substantial overprediction of end bearing by the PDA method relative to the q-z-derived values across all tested piles.

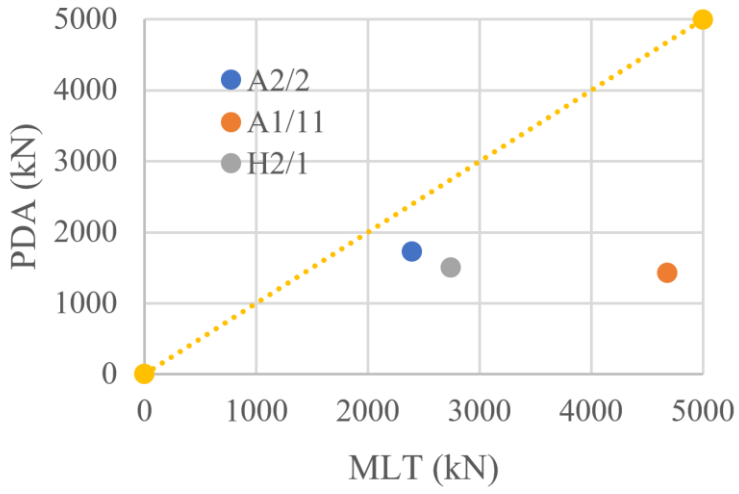

(a)

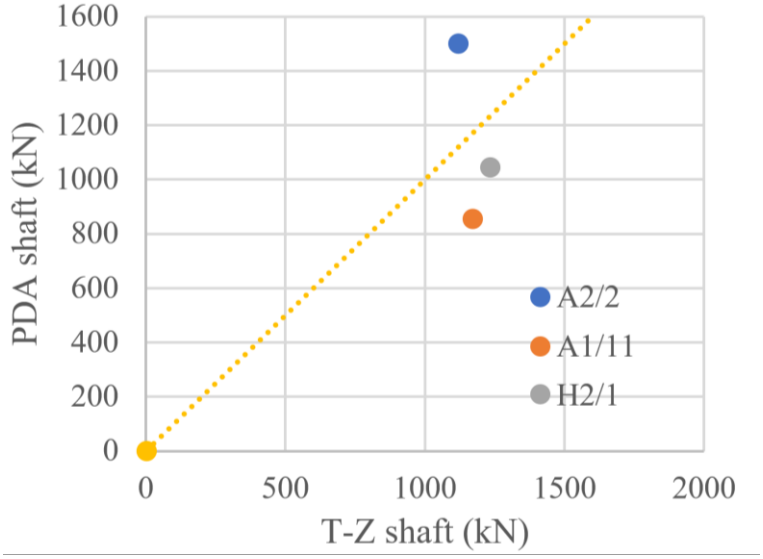

(b)

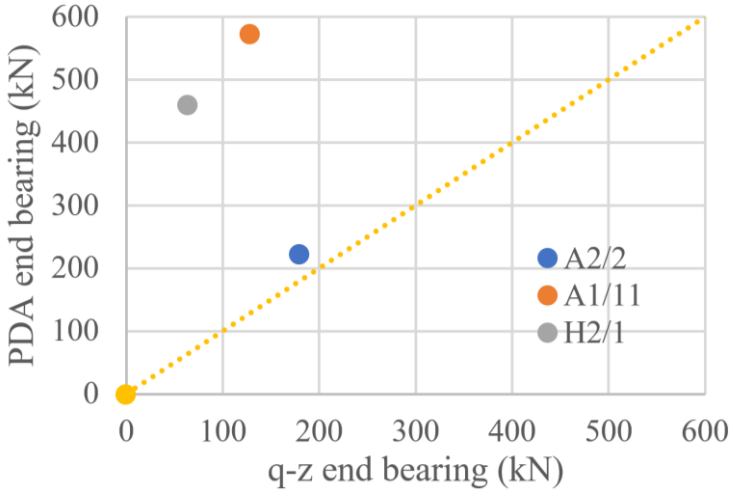

(c)

Figure 9. Comparisons between PDA estimates and other methods for micropiles: (a) Ultimate capacities from PDA vs. Chin's extrapolation from MLT, (b) Shaft friction from PDA vs. t-z back-analysis, (c) End bearing from PDA vs. q-z back-analysis

Table 5 presents PDA-derived capacities for three micropiles: A2-2 shows the highest total capacity at 1724 kN, primarily from shaft friction (1503 kN), surpassing A1/11 (856.4 kN) and H2/1 (1042 kN), while its end-bearing capacity (221 kN) is significantly lower than A1/11 (572.5 kN) and H2/1 (460.7 kN). These differences inform comparative analyses in Figure 8, highlighting variability in load distribution within karstic strata.

Table 5. Pile driving analyser (PDA) results

	A/2-2	A1/11	H2/1
Shaft capacity (kN)	1503.0	856.4	1042.0
End bearing capacity (kN)	221.0	572.5	460.7
Total (kN)	1724.0	1428.9	1502.7

The t-z and q-z back-analysis enhanced understanding by showing how load was transferred along the pile and how base resistance was engaged. Using static load test data, including strain gauge measurements, a load-transfer analysis was conducted. This involved calibrating t-z curves as shaft load-transfer relationships for different pile segments and a q-z curve (base load-settlement relationship) to match the measured load-settlement response. The analysis revealed the pile's internal behavior during loading: the load carried by upper soil (t-z in soil), rock socket (t-z in rock), and base (q-z). It confirmed that, despite being ignored in design, soil provided some friction, and the base resisted some load at higher loads, aligning with direct observations. This complements other results, as PDA cannot fully distinguish resistance sources, and raw static test data do not separate side and base resistance without additional measurements. The t-z/q-z analysis clarified load distribution, confirming that the rock socket carried most of the load, soil friction was minor, and base resistance contributed at peak load.

The t-z and q-z back-analysis aimed not to determine ultimate capacity but to evaluate pile performance under test loads and understand pile-ground interaction. It helps assess if the pile behaved as expected, calibrate soil and rock parameters, and predict behavior at higher loads by extending t-z and q-z curves, though extrapolation beyond tested loads is less reliable. Here, the analysis confirmed the conservative design's appropriateness, as mobilized rock socket friction remained below the assumed ultimate value, indicating extra capacity before failure. It provided insight into pile stiffness and resistance mobilization, showing settlement at working load and resistance contributions per layer. This supports serviceability and design refinement.

In summary, dynamic testing, static load testing, and load-transfer back-analysis together provide a consistent view of pile behavior. Soil friction and base resistance, ignored in design, contributed modestly, adding to the safety margin. Rock socket friction, the primary design component, was slightly lower than expected due to limited mobilization, epikarstic rock, construction factors, and scale effects. The higher capacity indicated by the Pile Driving Analyzer (PDA), the reliable performance demonstrated by the Maintained Load Test (MLT), and the detailed load distribution provided by the t-z/q-z back-analysis are consistent, each method evaluating distinct facets of pile behavior, namely ultimate capacity, serviceability under operational loads, and load transfer characteristics. Conservative design assumptions, like ignoring certain resistances or reducing rock friction, were validated, though actual behavior engaged all resistances to some extent. Geological factors and construction quality must be considered in predictions. The t-z and q-z analyses emphasize performance, ensuring acceptable settlement and safe load distribution at working loads, rather than focusing solely on ultimate capacity. This performance-based approach links design assumptions to field behavior, promoting safer, more economical foundation designs informed by real data.

The absence of direct stress distribution data limits precise separation of shaft friction and base stress; however, the CAPWAP analysis from PDA tests provided approximate distributions corroborated by t-z/q-z back-analysis. Future studies should incorporate vibrating wire strain gauges for enhanced accuracy.

5. Conclusions

In summary, the integrated testing and analysis program demonstrated that the test piles achieved load capacities well over the original design expectations, with relatively small settlements at the design proof load. The static maintained load tests showed that even at the maximum applied load of 1300 kN (the presumed design ultimate load), the piles exhibited only moderate settlements (9-10 mm) and did not reach failure. Extrapolation of the load-settlement curves using Chin's method indicated substantially higher ultimate capacities for all piles. For example, depending on the pile, the predicted ultimate capacity ranged from approximately 2400 kN up to 4700 kN, suggesting that the actual safety factor in the original design was relatively high. The high-strain dynamic (PDA) tests conducted on restrike yielded capacity estimates on the order of 1.4-1.7 MN, which, while lower than the static extrapolated values, still confirm that each pile's capacity exceeded the design nominal resistance (1300 kN) by a significant margin. The dynamic tests also provided a detailed look at load distribution: notably, a large portion of the resistance was mobilized in shaft friction along the overburden soil and weathered rock, a contribution the original design had conservatively neglected. The comparative analysis between measured behaviors and design predictions thus highlights that the design method, which assumed zero soil friction and relied only on rock socket capacity, was very conservative for these site conditions. All three piles sustained the full test load with minimal permanent deformation, reflecting robust

performance and indicating that additional load reserve was available beyond the test limit.

A key finding of this study is that even in karstic limestone terrain - where design practices often focus on end-bearing and socket friction in competent rock - the upper soil layers can provide non-negligible shaft resistance. Pile A2-2, for instance, in our tests, mobilized roughly 1.5 MN of shaft friction in the soil according to PDA results. In contrast, the design simulation had only anticipated 0.18 MN from the soil layer. This discrepancy explains the conservative nature of the original design predictions and underlines the value of empirical site testing. The presence of a void within the rock socket of pile A2-2 did not prevent that pile from achieving the highest capacity of the group; however, such features could influence the stiffness and load distribution, and their detection (through borehole coring in this case) is essential for proper interpretation of test results. Overall, the agreement in trend between the static and dynamic tests - both indicating capacities above the design value - provides confidence in the foundation performance. In contrast, the differences in absolute values emphasize the importance of using multiple methods to cross-verify pile capacity in complex ground conditions.

Based on the findings, it is recommended that designers consider incorporating site-specific test data for both static and dynamic loads to calibrate analytical models for pile behavior. Using t-z and q-z simulations calibrated to field tests can significantly improve the accuracy of predicted load-settlement performance and help optimize the design (for instance, by safely accounting for some skin friction in overburden soils when it is shown to be mobilized). For future projects in similar geologies, a combination of initial static load testing and PDA restrike testing on sacrificial test piles is advised to refine the design parameters, rather than assuming worst-case conditions. In terms of limitations, it should be noted that our static load tests were equipment-limited to 1300 kN, requiring extrapolation to assess ultimate capacity. This introduces some uncertainty, especially for the one pile (A1-11), where extrapolation suggested an extremely high capacity with a somewhat lower correlation fit. Moreover, dynamic test interpretations depend on wave propagation models and signal matching accuracy; factors such as strain rate effects and damping in rock sockets can affect the absolute values obtained. The study was also limited to three test piles at one site, which, while indicative, may not capture the full variability of karstic rock conditions or construction methods. Further research could involve testing a larger sample of piles with varying diameters and socket lengths to validate the observed trends. It would also be beneficial to investigate the long-term performance of such piles, via tension tests or sustained load tests, and to explore the effect of karst features on load transfer mechanisms in more detail. Despite these limitations, the current research provides a valuable case study demonstrating how combined static, dynamic, and simulation approaches can lead to a more robust understanding of pile capacity, and it underscores the efficacy of maintaining conservative design approaches while still leveraging test data to inform and optimize foundation solutions.

Acknowledgements

The authors would like to express their sincere appreciation to Universiti Malaysia Sarawak for providing the resources necessary to conduct this research. The authors would also like to thank Pasukan Project Khas 2 of Jabatan Kerja Raya Sarawak for facilitating access to the project site and providing technical information for the study.

REFERENCES

[1] Dotson D. W., Tarquinio F. S., "A Creative Solution to Problems with Foundation Construction in Karst," Geotechnical Special Publication, vol. 122, no. 1, pp. 627-634, 2003. DOI: 10.1061/40698(2003)57.

[2] Brown Dan A., T. J. P., Castelli Raymond J., Loehr Erik J., Drilled Shafts: Construction Procedures and Design Methods. Federal Highway Administration, 2018.

[3] Zhou W., Beck B. F., "Engineering Issues on Karst," Karst Management, vol. 1, no. 1, pp. 9-45, 2011. DOI: 10.1007/978-94-007-1207-2_2.

[4] Ballouz M., "Micropiling in Karstic Rock: New CMFF Foundation Solution Applied at the Sanita Factory," Geotechnical Special Publication, vol. 144, no. 1, pp. 1-11, 2005. DOI: 10.1061/40796(177)33.

[5] Traylor R. P., Cadden A. W., Bruce D. A., "High Capacity Micropiles in Karst: Challenges and Opportunities," Geotechnical Special Publication, vol. 116, no. 1, pp. 743-759, 2002. DOI: 10.1061/40601(256)53.

[6] Haberfield C. M., Lochaden A. L. E., "Analysis and Design of Axially Loaded Piles in Rock," Engineering Geology, vol. 253, no. 1, pp. 110-123, 2019. DOI: 10.1016/j.enggeo.2018.10.010.

[7] Shangxin F., Zhao Y., Wang Y., Wang S., Cao R., "A Comprehensive Approach to Karst Identification and Groutability Evaluation - A Case Study of the Dehou Reservoir, SW China," Engineering Geology, vol. 271, no. 1, pp. 1-14, 2020. DOI: 10.1016/j.enggeo.2020.105599.

[8] Budi G. S., Kosasi M., Wijaya D. H., "Bearing Capacity of Pile Foundations Embedded in Clays and Sands Layer Predicted Using PDA Test and Static Load Test," Procedia Engineering, vol. 125, no. 1, pp. 406-410, 2015. DOI: 10.1016/j.proeng.2015.11.101.

[9] Tan Y.C., Chow C.-M., "Foundation Design and Construction in Limestone Formation: A Malaysian Consultant's Experience," Proceedings of the International Symposium on Advances in Foundation Engineering

(ISAFE 2013), vol. 1, no. 1, pp. 1-26, 2013.

[10] Gue S.S., "Foundations in Limestone Areas of Peninsular Malaysia," Proceedings of the Civil and Environmental Engineering Conference (C&EEC) New Frontiers & Challenges, vol. 1, no. 1, pp. 1-10, 1999.

[11] Gómez J. E., Cadden A. W., Webster C. W., "Shallow Foundations in Karst: Limited Mobility Grout or Not Limited Mobility Grout," Geotechnical Special Publication, vol. 120, no. 1, pp. 1-12, 2003. DOI: 10.1061/40663(2003)83.

[12] Gutiérrez, F., Parise, M., De Waele, J., Jourde, H., "A Review on Natural and Human-Induced Geohazards and Impacts in Karst," Earth-Science Reviews, vol. 138, no. 1, pp. 61-88, 2014. DOI: 10.1016/j.earscirev.2014.08.002.

[13] Zerga, B., "Karst Topography: Formation, Processes, Characteristics, Landforms, Degradation and Restoration: A Systematic Review," Watershed Ecology and the Environment, vol. 6, no. 1, pp. 252-269, 2024. DOI: 10.1016/j.wsee.2024.01.001.

[14] Thierry, P., Debeblia, N., & Bitri, A., "Geophysical and Geological Characterisation of Karst Hazards in Urban Environments: Application to Orléans (France)," Bulletin of Engineering Geology and the Environment, vol. 64, no. 2, pp. 139-150, 2005. DOI: 10.1007/s10064-004-0270-6.

[15] Theilen-Willige, B., Malek, H. A., Charif, A., El Bchari, F., & Chaïbi, M., "Remote Sensing and GIS Contribution to the Investigation of Karst Landscapes in NW-Morocco," Geosciences, vol. 4, no. 2, pp. 50-72, 2014. DOI: 10.3390/geosciences4020050.

[16] Tan, B. K., Komoo, I., "Urban Geology: Case Study of Kuala Lumpur, Malaysia," Engineering Geology, vol. 28, no. 1-2, pp. 71-94, 1990. DOI:10.1016/0013-7952(90)90035-F.

[17] Tan, Y. C., Koo, K. S., Ting, D. I., "Deep Intervention Shaft Excavation in Kuala Lumpur Limestone Formation with Pre-Tunnelling Construction Method," Proceedings of the World Tunnel Congress 2019, vol. 1, no. 1, pp. 1-10, 2019.

[18] Parise, M., Lollino, P., "A Preliminary Analysis of Failure Mechanisms in Karst and Man-Made Underground Caves in Southern Italy," Geomorphology, vol. 134, no. 1-2, pp. 132-143, 2011. DOI: 10.1016/j.geomorph.2011.06.008.

[19] De Waele, J., Gutiérrez, F., Parise, M., Plan, L., "Geomorphology and Natural Hazards in Karst Areas: A Review," Geomorphology, vol. 134, no. 1-2, pp. 1-8, 2011. DOI: 10.1016/j.geomorph.2011.08.001.

[20] Stevanović, Z., Milanović, P., "Engineering Challenges in Karst," Acta Carsologica, vol. 44, no. 3, pp. 381-399, 2015. DOI: 10.3986/ac.v44i3.2578.